Double-slit, confinement, and non-Franck-Condon effects in photoionization of H_2 at high photon energy

J. Fernández,[1,*] O. Fojón,[2] and F. Martín[1]
[1]*Departamento de Química C-9, Universidad Autónoma de Madrid, 28049 Madrid, Spain*
[2]*Instituto de Física Rosario (CONICET-UNR) and Escuela de Ciencias Exactas (UNR), Pellegrini 250, 2000 Rosario, Argentina*
(Received 9 September 2008; published 18 February 2009)

A detailed theoretical study of H_2 ionization by photons of a few hundreds of eV is presented. Bound and continuum states are accurately evaluated by using *B*-spline basis functions. The nuclear degrees of freedom are also included. A striking feature is observed when one analyzes the vibrational distribution of the residual H_2^+ ion: this vibrational distribution does not follow the usual Franck-Condon behavior when H_2 is parallel to the polarization direction. The origin of this anomaly is related to interference effects. Such effects are more clearly seen in the fully differential electron angular distributions associated with specific vibrational states of H_2^+: for H_2 molecules perpendicular to the polarization direction, the distributions clearly resemble those obtained in Young's double-slit experiment, while, for molecules parallel to the polarization direction, they show that the electron is sometimes prevented to escape in the direction of the radiation field due to the suppression (or confinement) of a given partial wave. The calculations also show that, at these high photon energies, the nuclear asymmetry parameter exhibits a reminiscence of Cohen-Fano oscillations when it is plotted as a function of photon energy.

DOI: 10.1103/PhysRevA.79.023420 PACS number(s): 33.80.Eh

I. INTRODUCTION

Photoionization of H_2 is a recurrent topic in the literature since it is a benchmark to understand photoionization in more complicated molecules (see, e.g., Refs. [1,2] for a review). In particular, ionization produced by high-energy photons offers a very interesting perspective, since the wavelength λ_e of the ejected electron can be comparable to or smaller than the size of the molecule. In this case, the wave nature of the electron manifests through interferences and diffraction induced by the nuclei, similarly to what macroscopic waves do when they meet two macroscopic objects. More precisely, the size of H_2 is approximately given by its internuclear distance at equilibrium, R_e, which is 0.74 Å (i.e., 1.4 a.u). Therefore, such interferences are expected to show up when $\lambda_e \sim R_e$, i.e., for photon energies $h\nu \sim I_p + h^2/(2m_eR_e^2)$, where I_p is the vertical ionization potential, which is approximately 0.6 a.u., and where we have used the de Broglie relation $p_e = h/\lambda_e$. These energies correspond to photons of the order of a few hundred eV, i.e., to vacuum or extreme ultraviolet radiation, which is currently available in modern synchrotron radiation sources.

As predicted by Cohen and Fano in the sixties [3], a possible indication of the interferences associated with fast electron emission might already be seen in the integral photoionization cross section [4,5], which approximately follows the formula, in the fixed-nuclei approximation,

$$\sigma = \sigma_A \left[1 + \frac{\sin(k_e R)}{k_e R} \right], \tag{1}$$

where σ_A is the atomic photoionization cross section (for an effective charge Z_{eff}) and $k_e = 2\pi/\lambda_e$ is the electron wave vector. The signature of interferences is the oscillatory term within the brackets. However, due to the rapid decrease of σ_A with photon energy, i.e., with k_e, oscillations are usually observed in a rather indirect way, e.g., by dividing the total cross section by a "reasonable" independent estimate of σ_A [6,7] or by studying the ratio of two rapidly decreasing partial cross sections as in *K*-shell molecular photoionization [8]. An alternative way to uncover the expected oscillations, which is independent of the normalization procedure, is to analyze the forward-backward asymmetry of the electron emission [9].

In the last few years the idea of looking for two-center interferences in diatomic molecules has attracted the attention of scientists working in fields as diverse as high-order harmonic generation [10,11], tomographic imaging of molecular orbitals [12,13], or more traditional photoionization studies [14–18]. Inspired by the seminal work of Kaplan and Markin [19], Fernández *et al.* [17] have recently shown that a much clearer evidence of two-center interferences is obtained by analyzing the electron angular distributions arising from fixed-in-space molecules. This idea has been recently realized in COLTRIMS experiments [20] in which H_2 is doubly ionized by absorption of synchrotron radiation of about 200 eV. As reported in [17], these interferences critically depend on orientation. In particular, for molecules oriented parallel to the polarization direction, the angular distribution reveals a complex nodal structure when $k_eR \sim \ell\pi$, while for molecules oriented perpendicularly, typical Young's double-slit interferences are observed. Fernández *et al.* [17] also showed that the angular distributions change dramatically as the molecule vibrates, which means that the motion of fast electrons strongly depends on the nuclei's positions and, therefore, on the energy partitioning between electrons and nuclei. Similar conclusions were obtained in the case of H_2^+ photoionization.

In this paper, we extend the previous study of H_2 photoionization at high photon energies [17] by analyzing the vi-

*Present address: Lundbeck Foundation Theoretical Center for Quantum System Research, Department of Physics and Astronomy, University of Aarhus, 8000 Aarhus C, Denmark.

brational distribution of the remaining H_2^+ ion in the dominant nondissociative channel $H_2+\hbar\omega \rightarrow H_2^+(v)+e^-$. We also discuss in detail the various angular distributions that can be measured, such as the fully differential angular distribution (i.e., differential in the energy and direction of the ejected electron and the energy and orientation of the residual H_2^+ molecular ion), the angular distribution of the remaining H_2^+ ions irrespective of the electron ejection angle, and the electron angular distribution irrespective of the molecular orientation. The theoretical method used in [17] and in this work is described in detail in Sec. II. The results are presented and discussed in Sec. III. Conclusions and future perspectives are given in Sec. IV. In all cases, we restrict our study to linearly polarized light.

Atomic units are used throughout unless otherwise stated.

II. THEORETICAL METHODS

Photoionization cross sections have been evaluated in the framework of the dipole and the adiabatic Born-Oppenheimer (BO) approximations. The fully differential photoionization cross section, i.e., differential in both the energy and direction of the ejected electron and the energy and orientation of the residual H_2^+ molecular ion, is given by Dill's formula [21],

$$\frac{d\sigma_\alpha^{\mu_0}(\omega)}{d\Omega_n d\Omega_e d\varepsilon} = \frac{4\pi^2\omega}{c} \sum_{\mu_a,\mu_b} \sum_{\ell_a,m_a} \sum_{\ell_b,m_b} i^{(\ell_a-\ell_b)} e^{i[\hat{\sigma}_{\ell_b}(\varepsilon)-\hat{\sigma}_{\ell_a}(\varepsilon)]} (-1)^{m_b+\mu_a-\mu_0} T^*_{\alpha\ell_a m_a\mu_a}(\varepsilon) T_{\alpha\ell_b m_b\mu_b}(\varepsilon)$$
$$\times \sum_{L_e} \left[\frac{(2\ell_a+1)(2\ell_b+1)}{(2L_e+1)}\right]^{1/2} C(\ell_a,\ell_b,L_e;-m_a,m_b,M_e) C(\ell_a,\ell_b,L_e;0,0,0) Y^{M_e*}_{L_e}(\theta_e,\phi_e)$$
$$\times \sum_{L_\gamma} \left[\frac{1}{(2L_\gamma+1)}\right]^{1/2} C(1,1,L_\gamma;-\mu_a,\mu_b,M_\gamma) C(1,1,L_\gamma;-\mu_0,\mu_0,0) Y^{M_\gamma}_{L_\gamma}(\theta_n,\phi_n), \quad (2)$$

with $\mu_{a,b}=0,\pm1$, $M_\gamma=-\mu_a+\mu_b$, $M_e=-m_a+m_b$, $\ell_a+\ell_b \geqslant L_e \geqslant |\ell_a-\ell_b|$, and $2 \geqslant L_\gamma \geqslant 0$. In this equation, $\mu_0=0$ for linearly polarized light and $\mu_0=\pm1$ for circularly polarized light, α denotes the electronic state of the residual molecular ion, $\hbar\omega$ is the photon energy, ε is the photoelectron energy, $\Omega_e=(\theta_e,\phi_e)$ is the photoelectron emission direction in the molecular frame (θ_e and ϕ_e are the polar angles), $\Omega_n=(\theta_n,\phi_n)$ is the polarization direction with respect to the molecular axis z, c is the speed of light, $C(j_1,j_2,j;m_1,m_2,m)$ denotes a Clebsch-Gordan coefficient, Y_L^M is a spherical harmonic, $\hat{\sigma}_\ell(\varepsilon)$ is the Coulomb phase shift, and $T_{\alpha\ell m\mu}(\varepsilon)$ is the transition dipole matrix element given by

$$T_{\alpha\ell m\mu}(\varepsilon) = \int dR \langle \Psi^-_{\alpha v_\alpha \ell m\varepsilon}(\mathbf{r},R) | \mathbf{e}_\mu \cdot \mathbf{D} | \Psi_{gv}(\mathbf{r},R)\rangle, \quad (3)$$

where Ψ_{gv} is the ground molecular state of energy W_{gv}, $\Psi^-_{\alpha v_\alpha \ell m\varepsilon}$ is the final molecular state of energy $W_{v_\alpha}+\varepsilon$ representing a molecular ion in the v_α vibronic state (either dissociative or nondissociative) and an ionized electron of energy ε and angular momentum ℓm, $\mathbf{r}$ represents the electronic coordinates, R is the internuclear distance, $\mathbf{e}_\mu$ is the photon polarization vector, and $\mathbf{D}$ is either $\Sigma_i \mathbf{r}_i$ (length gauge) or $(\hbar\omega)^{-1}\Sigma_i \boldsymbol{\nabla}_i$ (velocity gauge). Energy conservation implies that $W_{gv}+\hbar\omega=W_{v_\alpha}+\varepsilon$. Neglecting rotational effects, the wave functions Ψ_{gv} and $\Psi^-_{\alpha v_\alpha \ell m\varepsilon}$ are evaluated in the adiabatic (Born-Oppenheimer, BO) approximation

$$\Psi_{nv_n}(\mathbf{r},R) = R^{-1}\chi_{v_n}(R)\psi_n(\mathbf{r},R), \quad (4)$$

where ψ_n and χ_{v_n} are the usual electronic and nuclear BO wave functions [1,2]. For each value of R, the electronic continuum states must satisfy the usual incoming boundary conditions of electron-molecule scattering [22] (see also [23]).

Integrating Eq. (2) over one or several differential magnitudes leads to partially differential or total cross sections, each one representing a specific experimental situation [24]. In particular, integrating Eq. (2) over the solid angle Ω_e leads to the cross section differential in the nuclear solid angle and in the energy of the ejected electron irrespective of the electron emission direction [24],

$$\frac{d\sigma_\alpha^{\mu_0}(\omega)}{d\Omega_n d\varepsilon} = \frac{1}{4\pi}\frac{d\sigma_\alpha^{\mu_0}(\omega)}{d\varepsilon}[1+\beta^{\mu_0}_{\alpha,n}(\varepsilon)P_2(\cos\theta_n)], \quad (5)$$

where P_2 is the Legendre polynomial of order 2, $d\sigma_\alpha^{\mu_0}(\omega)/d\varepsilon$ is the cross section differential in the energy of the ejected electron,

$$\frac{d\sigma_\alpha^{\mu_0}(\omega)}{d\varepsilon} = \frac{4\pi^2\omega}{3c}\sum_{\ell m\mu} |T_{\alpha\ell m\mu}(\varepsilon)|^2, \quad (6)$$

and $\beta^{\mu_0}_{\alpha,n}(\varepsilon)$ is the nuclear asymmetry parameter

$$\beta^{\mu_0}_{\alpha,n}(\varepsilon) = \frac{3\mu_0^2-2}{2}\frac{\sum_{\ell m\mu} |T_{\alpha\ell m\mu-M_i}(\varepsilon)|^2[3(m-M_i)^2-2]}{\sum_{\ell m\mu} |T_{\alpha\ell m\mu-M_i}(\varepsilon)|^2}, \quad (7)$$

where M_i is the projection of the initial-state angular momentum. As mentioned in the Introduction, in this paper we restrict our study to linearly polarized light, i.e., $\mu_0=0$, and

to H_2 molecules initially in the ground state $X^1\Sigma_g^+$, i.e., $M_i=0$. The above equations can also be used to obtain the cross sections differential in the energy of the residual molecular ion (nondissociative case) or the ejected proton (dissociative case) by using the energy conservation relation

$$W_{g\nu}+\hbar\omega=W_{\nu_\alpha}+\varepsilon \tag{8}$$

that relates ε to W_{ν_α}. Since the ground state of H_2 has $^1\Sigma_g^+$ symmetry, the dipole selection rule implies that only continuum states of $^1\Sigma_u^+$ and $^1\Pi_u$ symmetries can be populated. Hence, the cross section given in Eq. (6) can be written as the sum of $^1\Sigma_u^+$ and $^1\Pi_u$ cross sections,

$$\frac{d\sigma_\alpha(\omega)}{d\varepsilon}=\frac{d\sigma_\alpha^\Sigma(\omega)}{d\varepsilon}+2\frac{d\sigma_\alpha^\Pi(\omega)}{d\varepsilon}. \tag{9}$$

In this paper, we will analyze in detail two particular molecular orientations: parallel ($\theta_n=0$) and perpendicular ($\theta_n=\pi/2$) to the polarization vector. Hence, from Eq. (5), it can be easily seen that

$$\left.\frac{d\sigma_\alpha(\omega)}{d\varepsilon}\right|_{\theta_n=0}=\frac{\pi\omega}{c}\sum_\ell |T_{\alpha\ell 00}(\varepsilon)|^2\equiv\frac{1}{4\pi}\frac{d\sigma_\alpha^\Sigma(\omega)}{d\varepsilon} \tag{10}$$

and

$$\left.\frac{d\sigma_\alpha(\omega)}{d\varepsilon}\right|_{\theta_n=\pi/2}=\frac{\pi\omega}{c}\sum_\ell |T_{\alpha\ell 11}(\varepsilon)|^2\equiv\frac{1}{4\pi}\frac{d\sigma_\alpha^\Pi(\omega)}{d\varepsilon}. \tag{11}$$

Summation (integration) in Eqs. (9)–(11) over the energy of the ejected electron when the ionized molecule if left in a nondissociative (dissociative) state leads to the integrated cross section

$$\sigma_\alpha(\omega)\equiv \fint d\varepsilon\frac{d\sigma_\alpha^{\mu_0}(\omega)}{d\varepsilon}=\sigma_\alpha^\Sigma(\omega)+2\sigma_\alpha^\Pi(\omega) \tag{12}$$

and the corresponding ones for molecules oriented parallel and perpendicular to the polarization vector, respectively,

$$\sigma_\alpha(\omega)|_{\theta_n=0}=\frac{1}{4\pi}\sigma_\alpha^\Sigma(\omega) \tag{13}$$

and

$$\sigma_\alpha(\omega)|_{\theta_n=\pi/2}=\frac{1}{4\pi}\sigma_\alpha^\Pi(\omega). \tag{14}$$

The total photoionization cross section is obtained by summing over all open channels α the integrated cross sections given in Eq. (12),

$$\sigma(\omega)=\sum_\alpha \sigma_\alpha(\omega). \tag{15}$$

Starting again from Eq. (2), one can integrate over the solid angle Ω_n to obtain the cross section differential in the energy and solid angle of the ejected electron irrespective of the molecular orientation [25,26],

$$\frac{d\sigma_\alpha^{\mu_0}(\omega)}{d\Omega_e d\varepsilon}=\frac{1}{4\pi}\frac{d\sigma_\alpha^{\mu_0}(\omega)}{d\varepsilon}[1+\beta_{\alpha,e}^{\mu_0}(\varepsilon)P_2(\cos\theta_e)], \tag{16}$$

where $d\sigma_\alpha^{\mu_0}(\omega)/d\varepsilon$ is the cross section differential in the energy of the ejected electron given in Eq. (6) and $\beta_{\alpha,e}^{\mu_0}(\varepsilon)$ is the electron asymmetry parameter

$$\beta_{\alpha,e}^{\mu_0}(\varepsilon)=\frac{1}{5}\frac{C(1,1,2;-\mu_0,\mu_0,0)}{\sum_{\ell m\mu}|T_{\alpha\ell m\mu}(\varepsilon)|^2}\sum_{\mu_a,\mu_b}\sum_{\ell_a,m_a}\sum_{\ell_b,m_b} i^{(\ell_a-\ell_b)}e^{i(\hat\sigma_{\ell_b}(\varepsilon)-\hat\sigma_{\ell_a}(\varepsilon))}(-1)^{m_b+\mu_a}T^*_{\alpha\ell_a m_a\mu_a}(\varepsilon)T_{\alpha\ell_b m_b\mu_b}(\varepsilon)[(2\ell_a+1)(2\ell_b+1)]^{1/2}$$
$$\times C(\ell_a,\ell_b,2;-m_a,m_b,M_e)C(\ell_a,\ell_b,2;0,0,0)C(1,1,2;-\mu_a,\mu_b,M_\gamma)\delta_{m_a+\mu_a,m_b+\mu_b}. \tag{17}$$

The computational methods used to obtain the wave functions included in the $T_{\alpha\ell m\mu}$ matrix elements have been successfully applied to study a variety of different ionization problems in H_2, such as resonant dissociative photoionization [2,27,28] and ion impact ionization [29]. They have also led to the first numerical solution of the complete photoinduced breakup of H_2 [30]. More specifically, the vibrational (bound and dissociative) wave functions have been expanded in a basis of 280 B splines of order $k=8$ contained in a box of 12 a.u. The electronic wave functions have been evaluated as described in detail in Refs. [1,2]. Briefly, the ground state Ψ_g results from a configuration interaction (CI) calculation in which the H_2 Hamiltonian has been diagonalized in a basis of 321 configurations built from products of one-electron H_2^+ orbitals and pseudo-orbitals. The calculated energy at the equilibrium internuclear distance is −1.886 502 3 a.u., to be compared with the exact nonrelativistic value −1.888 761 38 a.u. [31]. All these orbitals have been represented through a one-center expansion that includes spherical harmonics up to $\ell=16$. The corresponding radial parts have been expanded in a basis of 310 B splines of order $k=8$ in a box of radial length of 60 a.u.

The final electronic continuum state $\Psi^-_{\alpha\nu_\alpha\ell m\varepsilon}$ results from a close coupling calculation that includes all partial waves with $\ell\leqslant 7$ associated with the four lowest ionization thresholds of H_2: $X^2\Sigma_g^+(1s\sigma_g)$, $^2\Sigma_u^+(2p\sigma_u)$, $^2\Pi_u(2p\pi_u)$, and $^2\Sigma_g^+(2s\sigma_g)$. For every value of R, these continuum states satisfy incoming boundary conditions corresponding to (i) one electron in a bound electronic state of H_2^+ and (ii) the other electron in a single outgoing spherical wave with a well-

defined value of the angular momentum ℓ plus a combination of incoming spherical waves for all accessible electronic states of H_2^+ and all possible values of the angular momentum of the ejected electron compatible with the molecular symmetry [1] (at the photon energy considered in this work, there is always a continuum state for each electronic state α of the residual H_2^+ ion and angular momentum ℓ of the ionized electron). Therefore, all calculated wave functions include electron correlation and the two-center character of the molecular potential. In addition, $\Psi^-_{\alpha v_\alpha \ell m \varepsilon}$ accounts for interferences among the various ionization thresholds and angular momenta of the ejected electron.

To check the convergence of the close coupling expansion, we have performed additional calculations (for a reduced number of photon energies) in which six additional ionization thresholds have been included [4]. No significant variations have been observed in the dominant $^2\Sigma_g^+(1s\sigma_g)$ channel. In the fixed-nuclei approximation, the error for this channel is typically smaller than 2.5%. The other channels will not be discussed in the paper because variations between the four- and ten-channel calculations can be as large as a factor of 2 depending on the photon energy. Interestingly, we have also found that, for the $^2\Sigma_g^+(1s\sigma_g)$ channel and for the highest photon energies reported in this work (i.e., for the highest electron energies), the first-order Born approximation to the final electronic continuum state $\Psi^-_{\alpha v_\alpha \ell m \varepsilon}$ is a reasonable approximation to evaluate both integrated and angle-differential photoionization cross sections. Nevertheless, all results reported below have been obtain from the full close-coupling calculation and not from the first-order Born approximation.

III. RESULTS

A. Integrated cross sections

In Fig. 1, we present the total photoionization cross section [as defined in Eqs. (12) and (15)] for H_2 as a function of photon energy. This cross section is the sum of the integrated cross sections over the four ionization channels included in our calculations. The total cross section is compared with that obtained in the fixed-nuclei approximation (FNA) [4]. As can be seen, the results of both calculations are very similar. At a photon energy ω of 2 a.u., they only differ by $\simeq$1–2%, whereas at ω=10 a.u. and 20 a.u., they differ by $\simeq$2% and $\simeq$6%, respectively. The agreement between the present results and those obtained in the FNA is similar for the partial $\Sigma_\alpha \sigma_\alpha^\Sigma$ and $2\Sigma_\alpha \sigma_\alpha^\Pi$ contributions (hereafter called Σ_u^+ and Π_u contributions or cross sections).

In Figs. 2 and 3, we present the contribution of each α ionization channel to the Σ_u^+ and Π_u cross sections. According to Eqs. (12)–(14), the Σ_u^+ and Π_u contributions are equal to 4π and 8π times the photoionization cross sections of H_2 parallel and perpendicular to the polarization vector, respectively. It can be seen that the first ionization limit is largely dominant for both final symmetries at all the photon energies studied. This is in agreement with our previous FNA results [4].

In Figs. 4 and 5, we present the contribution of the different partial waves associated with the lowest ionization channel $^2\Sigma_u^+(1s\sigma_g)$ for the $^1\Sigma_u^+$ and $^1\Pi_u$ final symmetries, respectively. These results are compared with those previously obtained by using the FNA [4]. Figure 5 shows that, for the $^1\Pi_u$ symmetry, the present results do not differ significantly from the FNA ones. The largest relative difference is observed for the ℓ=5 partial wave. There is also a slight difference for the ℓ=1 wave at high energies. Differences are more important in the case of the $^1\Sigma_u^+$ symmetry (see Fig. 4), in particular at photon energies where the ℓ=1 and ℓ=3 partial waves exhibit a minimum ($\sim$3.5 a.u. and $>$20 a.u., respectively). For photon energies around 3.5 a.u., the minimum observed for the ℓ=1 wave in the FNA results is much sharper and deeper than in the present calculations. A similar effect has been reported in the photoionization of H_2^+ [5]. In spite of this, the location of the minimum is barely affected

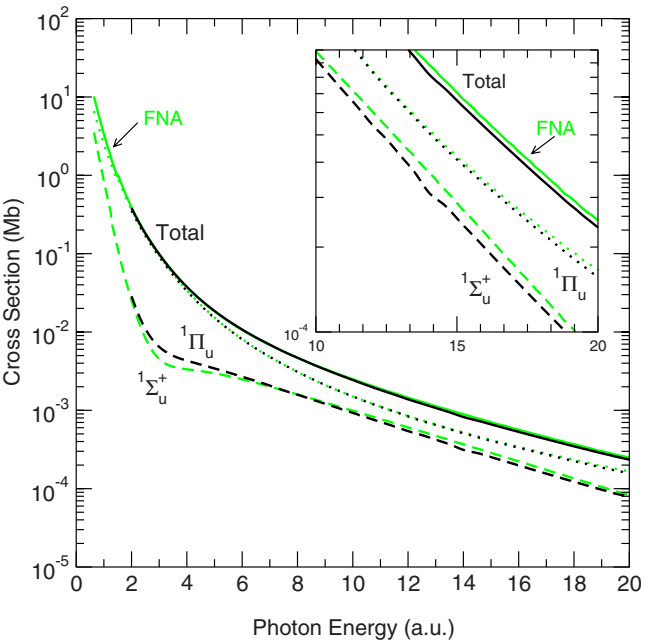

FIG. 1. (Color online) Total photoionization cross section of H_2 as a function of photon energy (full line). The partial Σ_u^+ and Π_u contributions (dashed and dotted lines, respectively) are also shown. Results from the FNA are shown in green.

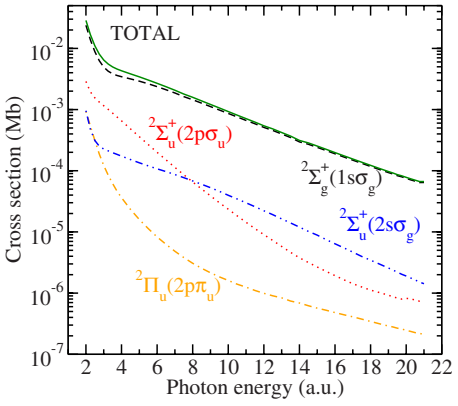

FIG. 2. (Color online) $^1\Sigma_u^+$ contribution to the total photoionization cross sections of H_2 as a function of photon energy. Contributions from the first four ionization thresholds are shown.

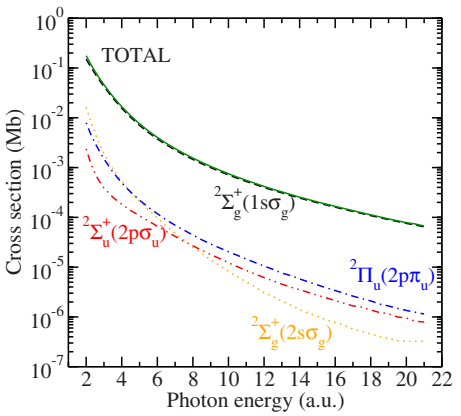

FIG. 3. (Color online) Same as in Fig. 2 for $^1\Pi_u$ contribution.

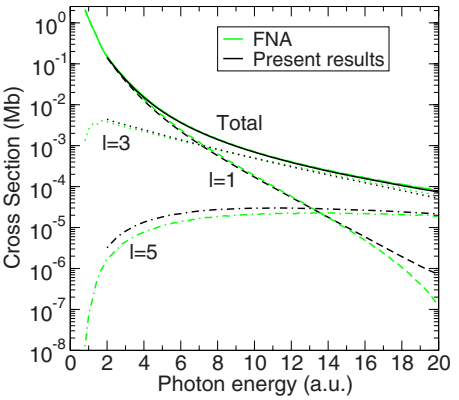

FIG. 5. (Color online) Same as in Fig. 4 for the $^1\Pi_u$ symmetry.

by the nuclear motion. As shown in our previous work [17], such minima are expected to appear when the momentum of the ejected electron satisfies the condition $k_eR_e \sim \ell\pi$. According to this simple formula, the minimum in the $\ell=1$ partial wave should appear at a photon energy of ~3.1 a.u. and that of the $\ell=3$ one at ~23 a.u. These values are in reasonable agreement with the actual ones observed in Fig. 4.

The electron energies, $k_e^2/2$, that result from replacing k_e by $\ell\pi/R_e$ coincide with those of an electron confined by a one-dimensional infinite-square well potential of size R_e. They also coincide, at high energies, with the minima of the transmission probability of an electron impinging on a one-dimensional potential formed by two δ functions separated by a distance R_e (these minima are due to destructive interference effects). The similarity of the $k_eR_e=\ell\pi$ rule with that obtained from these two models can be easily understood if one takes into account that, in the real three-dimensional world, the electrons tend to follow the oscillating electric field of the incidence radiation. As shown by Eq. (13), the $^1\Sigma_u^+$ cross section represents photoionization of H_2 molecules oriented parallel to the polarization axis, so that electrons are mostly forced to move along the internuclear axis. Since the ejected electron has a large kinetic energy, it will only be affected by the potential in the vicinity of the two nuclei, which is similar to what happens in a one-dimensional infinite-square well or in the scattering by two δ functions. Hence the larger k_e the more accurate the formula $k_eR_e \sim \ell\pi$. This is indeed what happens in H_2 photoionization even for the lowest value of k_e that arise from this formula ($\ell=1$) and also, as shown in [4,32], in H_2^+ photoionization.

The image of partial-wave confinement is further supported by a direct comparison between the calculated reduced electron continuum wave function and the H_2^+ molecular orbitals at $R_e=1.4$ a.u (the equilibrium internuclear distance of H_2). This is shown in Fig. 6. As can be seen, the

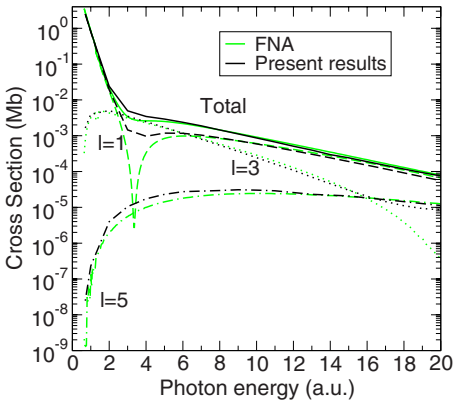

FIG. 4. (Color online) Partial wave contributions to the H_2 photoionization cross section associated with the $^2\Sigma_g^+(1s\sigma_g)$ ionization threshold. Results for $^1\Sigma_u^+$ symmetry. Results from the FNA are shown by red curves.

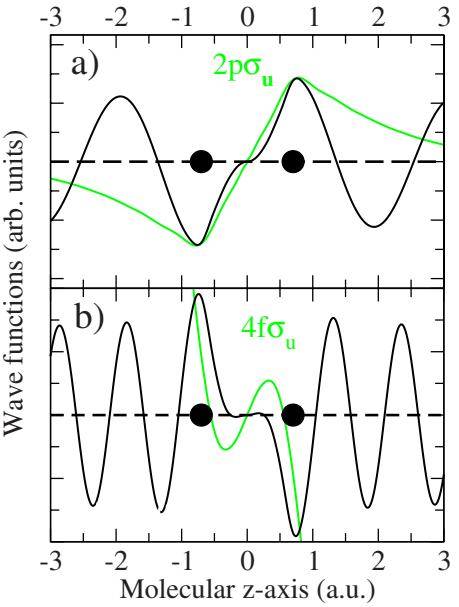

FIG. 6. (Color online) Wave functions of the ejected electron (black line) compared with the lowest H_2 molecular orbitals (green line) along the internuclear z axis for the k and ℓ values satisfying approximately the confinement condition. The wave functions of the ejected electron, obtained at the equilibrium distance, are the real K-matrix standing waves that correspond to the calculated complex S-matrix scattering wave functions. (a) $\varepsilon=2.6$ a.u. and $\ell=1$; (b) $\varepsilon=19$ a.u. and $\ell=3$.

reduced continuum wave function associated with the $\ell=1$ partial wave is very similar to the $2p\sigma_u$ orbital: not only does it have a node in the middle of the molecular axis but it also reproduces the maximum and the minimum of the $2p\sigma_u$ orbital at the nucleus positions. The reduced continuum wave function associated with the $\ell=3$ partial wave has a node, a maximum, and a minimum between the nuclei, exactly as in the $4p\sigma_u$ orbital, but the quantitative agreement is significantly worse. We have performed similar comparisons for H_2^+ (with $R_e=2$ a.u.) and the conclusions are the same [40].

The $k_eR_e \sim \ell\pi$ formula also arises naturally from a simplified one-dimensional version of the dipole transition matrix element given in Eq. (3), $\langle \sin(kz)|z|\psi_0\rangle$, in which the ejected electron is described by a plane wave and the initial molecular orbital ψ_0 is written as a linear combination of two $1s$ orbitals, $N[1s(\vec{r}+\frac{1}{2}R\hat{z})+1s(\vec{r}-\frac{1}{2}R\hat{z})]$ (see also [33]). This matrix element has minima at $kR=(2n+1)\pi$ and, since the dipole selection rule imposes odd parity in the final continuum state, it implies that ℓ must be strictly odd.

In Ref. [32], the minima in the $^1\Sigma_u^+$ cross section have been interpreted as Cooper-like minima similar to those found in atomic photoionization. However, there is nothing in the latter interpretation that allows one to predict that the minima in the cross section follow the formula $k_eR_e \sim \ell\pi$. In contrast, this formula arises naturally from any of the models mentioned above.

As we will see below, the fact that the contribution of a given partial wave significantly decreases at a very precise electron energy has important consequences in the electron angular distributions. It also has consequences in the vibrational distribution of the residual H_2^+ ion, which will not follow the expected Franck-Condon distribution.

B. Nondissociative photoionization

As mentioned in the Introduction, the energy of the absorbed photon can be shared between electrons and nuclei. In the nondissociative photoionization reaction, the residual H_2^+ molecular ion remains in the $^2\Sigma_g^+(1s\sigma)$ electronic state and can be left in any of its bound vibrational states (hereafter labeled by the vibrational quantum number v), so that the faster the ejected electron the lower the vibrational excitation of the residual H_2^+. This nondissociative process is by far the dominant contribution to the total cross section presented in the preceding section. The dissociative cross section is about two orders of magnitude smaller than the nondissociative one and, consequently, it is comparable to the double photoionization cross section associated with the complete break up of the H_2 molecule (see [30]). Therefore, couplings with the double ionization channels might significantly affect differential (but not integrated) cross sections associated with the dissociative single ionization channels. For this reason, we will only discuss differential cross sections for the nondissociative photoionization process.

At low photon energies (e.g., 20 eV), the vibrational distribution of H_2^+ follows approximately a Franck-Condon distribution, which predicts that the $v=2,3$ vibrational levels should be the most populated ones. We analyze now what happens at higher energies. Figures 7 and 8 show the calculated cross sections differential in the vibrational energy of the residual H_2^+ ion (viz. the reverse of the energy of the ejected electron) for the nondissociative case and for both parallel ($^1\Sigma_u^+$) and perpendicular ($^1\Pi_u$) molecular orientations, respectively.

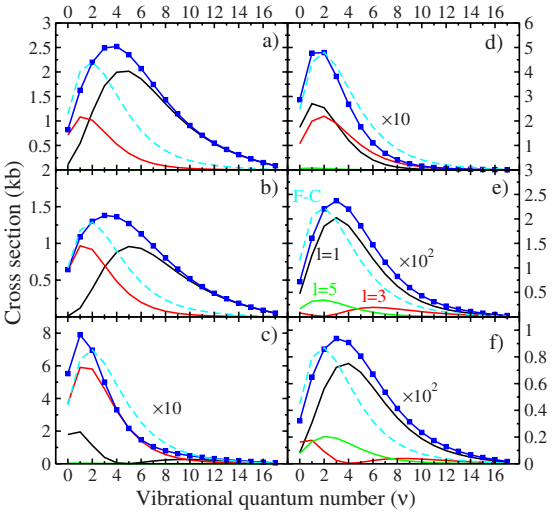

FIG. 7. (Color online) Nondissociative photoionization cross section of H_2 of $^1\Sigma_u^+$ symmetry, as a function of the vibrational quantum number v of the residual H_2^+ ion at photon energies 2, 2.5, 3.5, 6.0, 16.5, and 20 a.u., (a), (b), (c), (d), (e), and (f), respectively. Blue line with squares, total cross section; black line, $\ell=1$ partial wave contribution; red line, $\ell=3$; green line, $\ell=5$. Dashed cyan line, Frank-Condon distribution (FC).

Let us first consider the perpendicular case (final $^1\Pi_u$ symmetry) given in Fig. 8. It can be seen that, at all photon energies, the population of the final vibrational states follows a FC distribution. However, the relative contribution of the different partial waves does not follow such a simple behavior. At the lower photon energies, e.g., 2 and 5 a.u., the cross section is dominated by the $\ell=1$ partial wave (see Fig. 5) and Fig. 8 shows that this is the case for all the vibrational

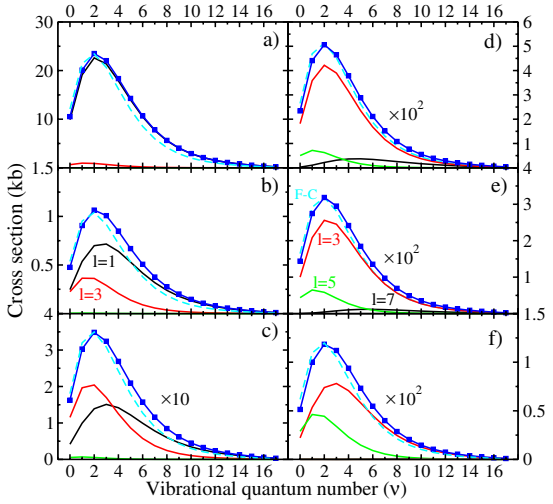

FIG. 8. (Color online) Same as Fig. 7 but for the $^1\Pi_u$ symmetry. Photon energies 2, 5, 7, 13, 15, and 20 a.u., panels (a), (b), (c), (d), (e), and (f), respectively.

states of the residual H_2^+ ion. As the photon energy increases, contribution of the $\ell=3$ partial wave becomes more and more important, but this increase is not uniform for all v and, therefore, the $\ell=3$ vibrational distribution does not follow the predictions of the FC approximation. For example, at a photon energy of 7 a.u. [Fig. 8(c)], the $\ell=3$ partial wave dominates for low v, while the $\ell=1$ one dominates at high v. At higher photon energy, e.g., 15 a.u. [Fig. 8(e)], the $\ell=3$ partial wave dominates for all v and at even higher photon energy, the $\ell=5$ partial contribution becomes progressively more important but again this increase is not uniform for all v (see, e.g., 20 a.u.).

The behavior is completely different for the parallel case (final $^1\Sigma_u^+$ symmetry, Fig. 7). First of all, the population of the final vibrational states does not follow a Franck-Condon behavior, even for a photon energy of 2 a.u. In this case, the $\ell=1$ partial wave dominates for almost all v, but, surprisingly, the $\ell=3$ partial wave dominates for the lowest v's. As the photon energy increases and one moves through the region where the $\ell=1$ partial wave has a minimum (see Fig. 4), the $\ell=3$ partial wave becomes dominant at higher and higher v until, at energies above 6 a.u., the $\ell=1$ partial wave becomes again the dominant one. A more careful inspection of Fig. 7 shows that the $\ell=1$ partial wave has a minimum around $v=5$ at a photon energy of 3.5 a.u. This is a photon energy that lies in the minimum of the cross section (see Fig. 4). Another minimum is clearly visible for the $\ell=5$ partial wave at photon energies of 16.5 and 20 a.u but now located around $v=4$. From this analysis it is thus clear that this deviation from the FC behavior is the consequence of the confinement effects discussed in the previous section.

C. Angular distribution of H_2^+ ions

We now analyze the angular distribution of the H_2^+ ions produced in the photoionization of H_2. The nuclear asymmetry parameter $\beta_{\alpha,n}^{\mu_0}(\varepsilon)$, which varies between -1 and 2, measures the relative importance of the parallel and perpendicular components of the electric dipole transition [24,34]. For $\beta_{\alpha,n}^{\mu_0}(\varepsilon)=2$ the H_2^+ angular distribution follows the polarization direction, for $\beta_{\alpha,n}^{\mu_0}(\varepsilon)=-1$ it is perpendicular to the polarization direction, and for $\beta_{\alpha,n}^{\mu_0}(\varepsilon)=0$ it is isotropic. As shown by Eq. (7), for a given photon energy, the asymmetry parameter depends on the electron energy (viz. the reverse of the vibrational energy of the residual H_2^+ ion). However, since the electron energy range in which the cross section is significantly different from zero is rather narrow (the FC region), variations of this parameter are only meaningful in that region. We have found that even in this narrow region, the asymmetry parameter associated with the lowest ionization channel $^2\Sigma_g^+(1s\sigma_g)$ varies significantly with the vibrational quantum number of the residual H_2^+ ion. This variation depends strongly on the photon energy.

Nevertheless, very often, the experiments do not resolve the dependence with the electron energy. In this case, one has to integrate Eq. (5) over electron energy, leading to

$$\frac{d\sigma_\alpha^{\mu_0}(\omega)}{d\Omega_n} = \frac{\sigma_\alpha^{\mu_0}(\omega)}{4\pi}[1+\beta_{\alpha,n}^{\mu_0}P_2(\cos\theta_n)], \tag{18}$$

where $\beta_{\alpha,n}^{\mu_0}$ is the average asymmetry parameter

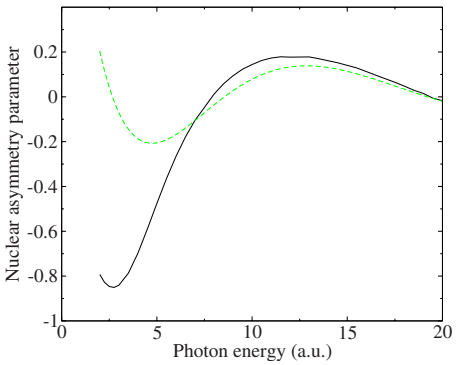

FIG. 9. (Color online) Nuclear asymmetry parameter for the $^2\Sigma_g^+(1s\sigma_g)$ channel as a function of photon energy. Black line, present results; dashed green line, the $1+\sin(k_eR)/k_eR$ curve (shifted vertically) taken from Ref. [4].

$$\beta_{\alpha,n}^{\mu_0} = \sum\!\!\!\!\!\!\int d\varepsilon \frac{d\sigma_\alpha^{\mu_0}(\omega)}{d\varepsilon}\beta_{\alpha,n}^{\mu_0}(\varepsilon) \tag{19}$$

and $\sigma_\alpha^{\mu_0}(\omega)$ is the integrated cross section given in Eq. (12).

Figure 9 shows the average nuclear asymmetry parameter associated with the lowest ionization channel $\alpha=^2\Sigma_g^+(1s\sigma_g)$ considered in this work. As can be seen, the asymmetry parameter oscillates with photon energy. This is a reminiscence of the Cohen-Fano oscillations. Indeed, from Eq. (7), the β parameter can be written

$$\beta_{\alpha,n}^{\mu_0} = 2\frac{\sigma_\alpha^{\Sigma}-\sigma_\alpha^{\Pi}}{\sigma_\alpha}, \tag{20}$$

which shows that it is proportional to the ratio of the Σ-Π difference and the integrated cross section. Since the latter varies rather monotonically with photon energy, while the former emphasizes the nonmonotonic behavior of the Σ contribution, this results in the observed oscillations. It can be seen that, as expected from the Cohen-Fano model [see Eq. (1)], these oscillations qualitatively follow the behavior $1+\sin(k_eR)/k_eR$. An interesting conclusion that can be obtained from this analysis is that Cohen-Fano oscillations could directly be observed in experiments through the analysis of the nuclear asymmetry parameter thus avoiding the ambiguity associated with the use of atomic cross sections σ_A needed to obtain the σ/σ_A ratio [see Eq. (1)]. The price to pay is that the orientation of the remaining H_2^+ molecular ion should be determined, something that is not obvious by using the current COLTRIMS devices.

D. Angular distribution of electrons

We first investigate the electron angular distributions irrespective of the molecular orientation. For this purpose, we have evaluated the electron asymmetry parameter. As for the nuclear asymmetry parameter presented in the previous section, the experiments do not resolve the dependence with the electron energy. Thus, one has to integrate Eq. (16) over electron energy, leading to

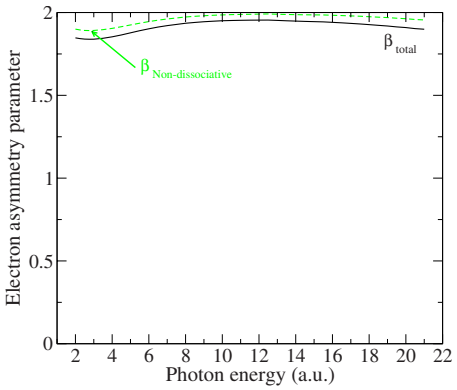

FIG. 10. (Color online) H_2 electron asymmetry parameter as a function of photon energy. Black line, present result; green dashed line, nondissociative contribution.

$$\frac{d\sigma_\alpha^{\mu_0}(\omega)}{d\Omega_e} = \frac{\sigma_\alpha^{\mu_0}(\omega)}{4\pi}[1 + \beta_{\alpha,e}^{\mu_0} P_2(\cos\theta_e)], \tag{21}$$

where $\beta_{\alpha,e}^{\mu_0}$ is the average asymmetry parameter

$$\beta_{\alpha,e}^{\mu_0} = \sum\!\!\!\!\!\!\int d\varepsilon \frac{d\sigma_\alpha^{\mu_0}(\omega)}{d\varepsilon} \beta_{\alpha,e}^{\mu_0}(\varepsilon) \tag{22}$$

and $\sigma_\alpha^{\mu_0}(\omega)$ is the integrated cross section given in Eq. (12).

Figure 10 shows the average electron asymmetry parameter associated with the $^2\Sigma_g^+(1s\sigma_g)$ ionization channel. As can be seen, the value of this asymmetry parameter is close to 2 in the whole photon energy range, either including or excluding the dissociative channels. Some oscillations with photon energy can also be observed, but, in contrast with the nuclear asymmetry parameter, their amplitude is very small and, therefore, they will be hard to detect experimentally. We have also studied the variation with electron energy of the nonaveraged asymmetry parameter and we have found that $\beta_{\alpha,e}^{\mu_0}(\varepsilon)$ is close to 2 irrespective of the electron energy (viz. the reverse of the vibrational energy of the residual H_2^+ ion). This means that, for randomly oriented molecules, the electrons escape parallel to the polarization vector irrespective of their energy. As a result of the mixing between the different molecular orientations, any trace of the interference effects discussed in the previous sections is lost.

A much richer information can be obtained from the electron angular distributions from fixed-in-space molecules. Figures 11–13 show the electron angular distributions for nondissociative photoionization of H_2 at a photon energy of 2.5, 6.0, and 13.0 a.u., respectively. The three figures include results for molecules parallel (Σ_u^+ symmetry) and perpendicular (Π_u symmetry) to the polarization direction. The corresponding angular distributions are only shown for the case of H_2^+ ions left in the $v=0$, 2, 4, and 12 vibrational levels. The first three values of v correspond to vibrational levels that are close to or within the FC region, while the $v=12$ vibrational level is clearly outside this region.

For the perpendicular orientation, one can see that, in all cases, the electronic emission is mainly produced, as expected, in the direction of the polarization vector. At a photon energy of 13 a.u. (see Fig. 13), the angular distributions

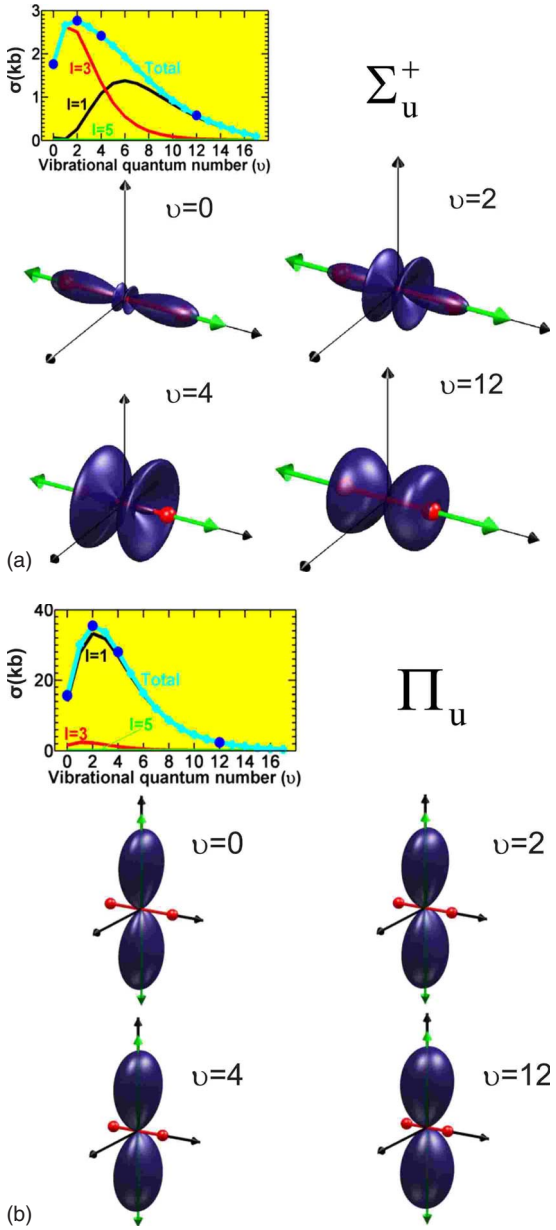

FIG. 11. (Color online) Electron angular distributions for nondissociative photoionization $[H_2+\hbar\omega \rightarrow H_2^+(v)+e^-]$ of H_2 oriented parallel (Σ_u^+ symmetry) and perpendicular (Π_u symmetry) to the polarization direction. Angular distributions corresponding to leaving the residual H_2^+ ion in different vibrational states are shown by three-dimensional plots in blue. For a better visualization, these distributions have been renormalized so that their maximum value is always 1. The polarization direction is indicated by the double arrow (green). The two nuclei are indicated by two small spheres (red). The angle-integrated cross sections, including the partial wave decomposition, as a function of the final quantum vibrational number v are shown in the two-dimensional plots. All results obtained at a photon energy of 2.5 a.u.

exhibit smaller lobes in other directions. These are typical diffraction patterns produced by a double slit. Indeed, at 13 a.u., the wavelength of the ejected electron is already smaller (1.26 a.u.) than the molecule internuclear distance (1.4 a.u.) and, consequently, diffraction from the two centers

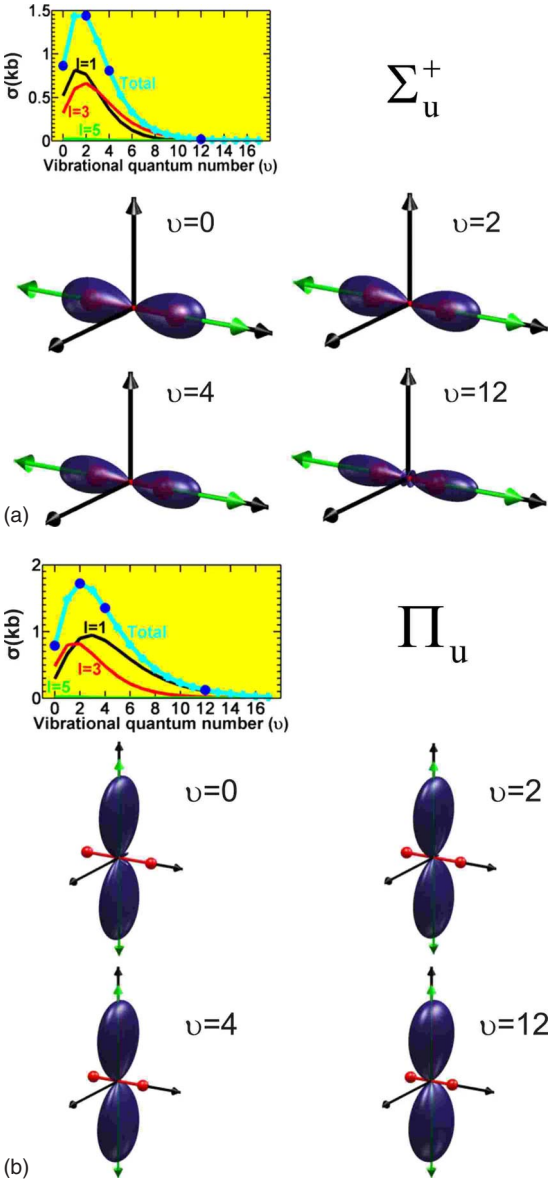

FIG. 12. (Color online) Same as Fig. 11 but at a photon energy of 6.0 a.u.

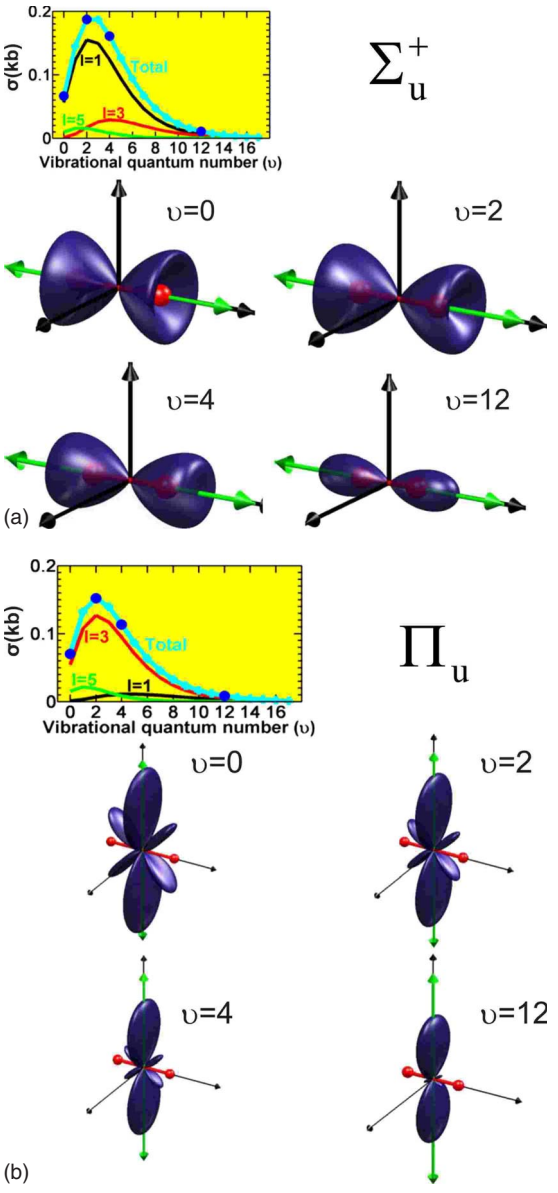

FIG. 13. (Color online) Same as Fig. 11 but at a photon energy of 13.0 a.u.

is expected to lead to constructive interferences at specific directions of the ejected electron as given by Young's formula $R \sin \theta_e = n\lambda_e$. Similar findings have been reported in [17] for other photon energies and for photoionization of H_2^+. As can be seen in Fig. 13, the relative intensity of the additional lobes increases as the vibrational energy of the residual H_2^+ ion decreases (or equivalently, as the electron emission energy increases). We will come back later to this specific point. It is worth noticing that very small additional lobes also exist at a photon energy of 6 a.u., although they are barely observed in Fig. 12. At this photon energy, the wavelength of the ejected electron is still significantly larger (1.9 a.u.) than the molecule internuclear distance.

In the parallel case and for a photon energy of 2.5 a.u. (see Fig. 11), the angular distribution exhibits completely different features. The distribution has an almost perfect f shape ($\ell=3$) when H_2^+ remains in a low vibrational level. As the vibrational quantum number of the remaining H_2^+ increases, a complicated angular pattern emerges as the result of the interference between the $\ell=1$ and $\ell=3$ partial waves. For $v=4$, interferences lead to almost no emission in the direction of the polarization vector, whereas, for $v=12$, the distribution is almost p like. In Ref. [17], this sudden change of the angular distribution with v has been attributed to partial-wave confinement because, around this photon energy, the $\ell=1$ partial component of the $^1\Sigma_u^+$ integrated cross section exhibits a pronounced minimum (see Fig. 4). At a photon energy of 6.0 a.u. (see Fig. 12), the angular distribution exhibits a typical p-like pattern irrespective of the final vibrational state of the residual H_2^+ ion. At this photon energy, we are far from any of the minima shown in Fig. 4 and, consequently, no effects due to partial wave confinement are expected to appear. However, at a photon energy of 13.0 a.u., non-p-like distributions are observed again at the lowest values of v.

As mentioned above, partial wave confinement appears when the energy of the ejected electron approximately satisfies the formula $k_e R \sim \ell\pi$, where R is now the value of the internuclear distance at which the electron emission occurs. The problem in nondissociative photoionization of H_2 is that the molecule is vibrating in both the initial and the final states and, therefore, it is not straightforward to define unambiguously the value of R that must be used in the former equation. In order to better understand the origin of this effect in H_2, it is useful to compare the present situation with that of H_2^+ photoionization. In the latter case, there is an almost perfect one-to-one mapping between the energy of the residual ion and R [17] because electron emission is followed by the Coulomb explosion of the remaining protons. Assuming that the protons behave classically, it is then possible to relate the observed proton kinetic energy to the R value at which Coulomb explosion takes place, $2E_{H^+} \sim 1/R$ [35]. This is usually called *the reflection approximation*. In H_2 photoionization, one cannot invoke the reflection approximation because the remaining molecular ion is left in a bound vibrational state. However, according to previous work [36,37], one can expect that different vibrational states of the residual ion sample a narrow enough subset of R values, so that the above picture still remains approximately valid. We have checked that this is the case at the highest photon energies (e.g., 13 a.u.) if R is chosen around the inner classical turning point associated with the final vibrational state of the residual H_2^+ ion. For the $v=0$, 2, 4, and 12 vibrational levels of the residual H_2^+ ion, the inner classical turning points are $R_{in}=1.71$, 1.46, 1.34, and 1.15 a.u., respectively. For a photon energy of 13 a.u., it can be easily seen that the condition for suppression of the $\ell=3$ partial wave, $R=3\pi/k_e$, leads to $R=1.8$ a.u., which is close to the classical turning associated with $v=0$. This is the reason why the corresponding angular distribution shown in Fig. 13 exhibits a pattern that reminds us of confinement. A similar argument explains why there is no such effect for any v at a photon energy of 6 a.u. and why it appears around $v=2$ when the photon energy is 2.5 a.u. (in this case for the $\ell=1$ partial wave). Among the three chosen photon energies, the predictive value of the model is worse at 2.5 a.u. because the electron energy is not high enough.

In the case of H_2^+ photoionization, the angular distributions approximately follow the formula [38] $(\mathbf{e}_\mu \cdot \mathbf{k}_e)^2 \cos^2(\mathbf{k}_e \cdot \mathbf{R}/2)$. If $\mathbf{e}_\mu$ and $\mathbf{k}_e$ are parallel to the molecular axis, this formula leads to zero when $k_e R = \pi, 3\pi, \ldots$, i.e., no electron emission along the molecular axis in agreement with the image of partial wave confinement. A similar formula describes in classical optics the interference produced at long distances by two radiating dipole antennas separated a distance R. For H_2, the predictive value of the above model is more limited because one cannot rely on the reflection approximation to deduce the value of R and electron correlation can introduce some distortions. However, we have checked that the formula still works at the highest photon energies if one uses again for R the values of the inner classical turning points associated with the H_2^+ vibrational levels. This is illustrated in Fig. 14 for both the parallel and the perpendicular orientations and for a photon energy of 13 a.u.. As can be seen, the observed trends closely follow those of the angular distributions shown in Fig. 13. Nevertheless, the quantitative value of the model rapidly deteriorates as the photon energy decreases, especially in the case of parallel orientation where changes in the angular distribution are more abrupt. In particular, at 2.5 a.u., it fails in predicting the shape of the angular distributions presented in Fig. 11 for the parallel orientation and for low v.

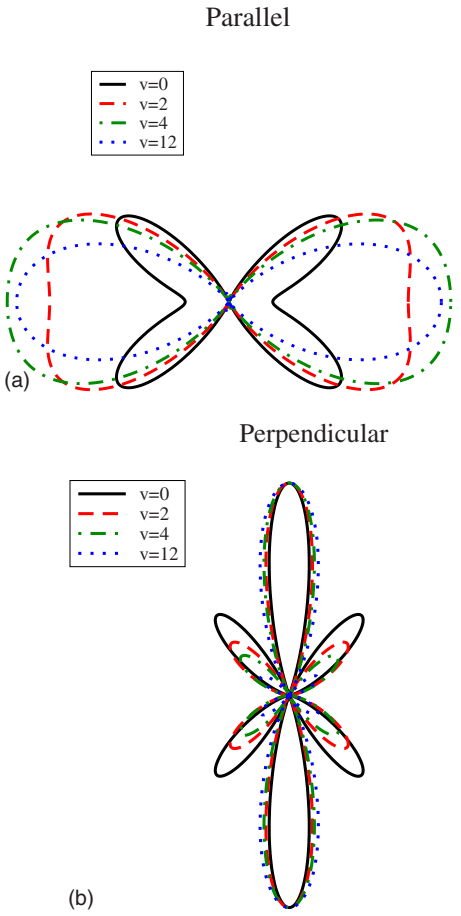

FIG. 14. (Color online) Angular distributions at a photon energy of 13 a.u. that result from the model of Ref. [38] by using the inner classical turning points associated with the $v=0$, 2, 4, and 12 vibrational levels of H_2^+.

IV. CONCLUSION

We have presented a detailed theoretical study of H_2 ionization by photons of a few hundred eV. The calculations, performed in the framework of the Born-Oppenheimer approximation, include the effect of the nuclear motion and make use of B-spline functions to evaluate bound and continuum states. In the case of molecules oriented parallel to the polarization direction, the partial-wave contributions to the integrated cross sections exhibit pronounced minima at electron energies that closely follow the relationship $k_e R_e \sim \ell\pi$, where R_e is the equilibrium internuclear distance. As discussed in Ref. [17], this is due to partial-wave confinement of the ejected electron. For molecules oriented perpendicular to the polarization direction, the integrated cross section varies smoothly with electron energy. These conclusions

agree with those obtained previously in the framework of the fixed-nuclei approximation.

From the analysis of the vibrational distribution of the remaining H_2^+ ion in the dominant nondissociative reaction $H_2+\hbar\omega \rightarrow H_2^+(v)+e^-$, we conclude that, for molecules parallel to the polarization direction, the calculated distribution does not follow a typical Franck Condon (FC) distribution. Deviations from the FC distribution are more pronounced in the regions where $k_eR_e \sim \ell\pi$. In contrast, for molecules perpendicular to the polarization direction, the vibrational distribution closely follow an FC distribution at all photon energies.

We have also discussed in detail the various angular distributions that can be measured. The fully differential angular distribution (i.e., differential in the energy and direction of the ejected electron and the energy and orientation of the residual H_2^+ molecular ion), clearly exhibit the effects of partial-wave confinement and Young's double slit interferences for molecules that are, respectively, parallel and perpendicular to the polarization direction. Again, the former effect appears when $k_eR=\ell\pi$, where R is approximately the value of the internuclear distance at the inner classical turning point associated with the vibrational level of the residual H_2^+ ion. Young's double-slit interferences are clearly visible in the perpendicular case when the electron wavelength is comparable to the internuclear distance. For a given photon energy, the latter interference varies with the energy of the ejected electron and this variation is reasonably described by the model of Ref. [38], $(\mathbf{e}_\mu\cdot\mathbf{k}_e)^2\cos^2(\mathbf{k}_e\cdot\mathbf{R}/2)$, assuming again that R is the value of the internuclear distance at the inner classical turning point associated with the vibrational level of the residual H_2^+ ion.

From the analysis of the angular distribution of the remaining H_2^+ ions irrespective of the electron ejection angle (suggested, e.g., in Ref. [39]), we have concluded that Cohen-Fano oscillations are observed when the corresponding nuclear asymmetry parameter is plotted as a function of photon energy. This provides a direct way of observing such oscillations without the need for atomic photoionization cross sections that would be needed to uncover the oscillations hidden in Eq. (1) due to the rapid decrease of the molecular cross section with photon energy. In contrast, the analysis of the electron angular distribution irrespective of the molecular orientation does not provide too much information since the corresponding asymmetry parameter is close to 2 in the whole range of photon energies investigated in this work.

In spite of this progress, there still remain some open questions, in particular when the photon energy is further increased. In this case, the validity of the dipole approximation to evaluate the transition matrix elements is doubtful and future theoretical work should include higher multipole contributions. It also would be interesting to analyze how the mentioned effects appear when one considers other orientations of the molecular target and not only the parallel and perpendicular cases discussed in this work. Finally, recent experiments in H_2 double photoionization with circularly polarized light [20] raise the question of how these simple physical effects manifest with this particular polarization.

ACKNOWLEDGMENTS

This work was partially supported by the Spanish Ministerio de Ciencia e Innovación (Contract No. FIS2007-60064), the European Science Foundation (COST Action No. CM0702), and the Spanish Subdirección General de Cooperación Internacional. O.F. acknowledges the kind hospitality in the group of "Computations in Atomic and Molecular Physics of Unbound Systems" of the Universidad Autónoma de Madrid (Spain), as well as financial support from the Secretaría de Estado de Educación y Universidades (Spain) through a grant. Calculations were performed at the Barcelona Supercomputer Center Mare Nostrum and the Centro de Computación Científica UAM (Spain).

[1] F. Martín, J. Phys. B **32**, R197 (1999).
[2] H. Bachau, E. Cormier, P. Decleva, J. E. Hansen, and F. Martín, Rep. Prog. Phys. **64**, 1815 (2001).
[3] H. D. Cohen and U. Fano, Phys. Rev. **150**, 30 (1966).
[4] O. A. Fojón, J. Fernández, A. Palacios, R. D. Rivarola, and F. Martín, J. Phys. B **37**, 3035 (2004).
[5] O. A. Fojón, A. Palacios, J. Fernández, R. D. Rivarola, and F. Martín, Phys. Lett. A **350**, 371 (2006).
[6] N. Stolterfoht *et al.*, Phys. Rev. Lett. **87**, 023201 (2001).
[7] D. Misra, U. Kadhane, Y. P. Singh, L. C. Tribedi, P. D. Fainstein, and P. Richard, Phys. Rev. Lett. **92**, 153201 (2004).
[8] X. J. Liu *et al.*, J. Phys. B **39**, 4801 (2006).
[9] D. Misra, A. Kelkar, U. Kadhane, A. Kumar, L. C. Tribedi, and P. D. Fainstein, Phys. Rev. A **74**, 060701(R) (2006).
[10] M. Lein, P. P. Corso, J. P. Marangos, and P. L. Knight, Phys. Rev. A **67**, 023819 (2003).
[11] G. L. Kamta and A. D. Bandrauk, Phys. Rev. A **71**, 053407 (2005).
[12] J. Itatani, J. Levesque, D. Zeidler, H. Niikura, H. Pépin, J. C. Kieffer, P. B. Corkum, and D. M. Villeneuve, Nature (London) **432**, 867 (2004).
[13] M. Meckel *et al.*, Science **320**, 1478 (2008).
[14] S. N. Yurchenko, S. Patchkovskii, I. V. Litvinyuk, P. B. Corkum, and G. L. Yudin, Phys. Rev. Lett. **93**, 223003 (2004).
[15] D. Rolles *et al.*, Nature (London) **437**, 711 (2005).
[16] D. Toffolli and P. Decleva, J. Phys. B **39**, 2681 (2006).
[17] J. Fernández, O. Fojón, A. Palacios, and F. Martín, Phys. Rev. Lett. **98**, 043005 (2007).
[18] F. L. Yip, C. W. McCurdy, and T. N. Rescigno, Phys. Rev. A **78**, 023405 (2008).
[19] I. G. Kaplan and A. P. Markin, Sov. Phys. Dokl. **14**, 36 (1969).
[20] D. Akoury *et al.*, Science **318**, 949 (2007).
[21] D. Dill, J. Chem. Phys. **65**, 1130 (1976).
[22] G. Breit and H. A. Bethe, Phys. Rev. **93**, 888 (1954).
[23] R. G. Newton, *Scattering Theory of Waves and Particles* (McGraw Hill, New York, 1966).

[24] S. Wallace and D. Dill, Phys. Rev. B **17**, 1692 (1978).
[25] J. C. Tully, R. S. Berry, and B. J. Dalton, Phys. Rev. **176**, 95 (1968).
[26] I. Cacelli, V. Carravetta, A. Rizzo, and R. Moccia, Phys. Rep. **205**, 283 (1991).
[27] I. Sánchez and F. Martín, Phys. Rev. Lett. **82**, 3775 (1999).
[28] F. Martín *et al.*, Science **315**, 629 (2007).
[29] G. Laurent *et al.*, Phys. Rev. Lett. **96**, 173201 (2006).
[30] W. Vanroose, F. Martín, T. N. Rescigno, and C. W. McCurdy, Science **310**, 1787 (2005).
[31] W. Kołos, K. Szalewicz, and H. J. Monkhorst, J. Chem. Phys. **84**, 3278 (1986).
[32] R. Della Picca, P. D. Fainstein, M. L. Martiarena, and A. Dubois, Phys. Rev. A **77**, 022702 (2008).
[33] N. Sisourat, J. Caillat, A. Dubois, and P. D. Fainstein, Phys. Rev. A **76**, 012718 (2007).
[34] J. Fernández, Ph.D. thesis, Universidad Autónoma de Madrid, 2008.
[35] T. Weber *et al.*, Nature (London) **431**, 437 (2004).
[36] J. L. Dehmer, D. Dill, and S. Wallace, Phys. Rev. Lett. **43**, 1005 (1979).
[37] T. Jahnke *et al.*, Phys. Rev. Lett. **93**, 083002 (2004).
[38] M. Walter and J. Briggs, J. Phys. B **32**, 2487 (1999).
[39] X. J. Liu, R. R. Lucchese, A. N. Grum-Grzhimailo, Y. Morishita, N. Saito, G. Prümper, and K. Ueda, J. Phys. B **40**, 485 (2007).
[40] In Ref. [32], the continuum wave functions of H_2^+, were only compared with the $1s\sigma_g$, orbital, which does not have the correct nodal symmetry imposed by the dipole selection rule.